Microstructure Evolution and Interface Stability of Thermal Barrier Coatings with Vertical Type Cracks in Cyclic Thermal Exposure

Zhe Lu, Sang-Won Myoung, Hyun-Sung Kim, Min-Sik Kim, Je-Hyun Lee, Yeon-Gil Jung, Jung-Chel Jang, and Ungyu Paik

In this study, the effects of intrinsic feature of microstructure in thermal barrier coatings (TBCs) with and without vertical cracks on the microstructure and mechanical properties were investigated in cyclic thermal exposure. The hardness values of TBCs with vertical cracks were higher than those without vertical cracks, showing a good agreement with microstructure. The TBC prepared without vertical cracks using the 204-NS was delaminated after 250 cycles in the cyclic thermal exposure test. The TBCs with and without vertical cracks prepared with 204 C-NS and the TBC with vertical cracks prepared with 204 NS showed a sound condition without any cracking at the interface or spalling of top coat. After the thermal exposure of 381 cycles, the hardness values were increased in the survived TBC specimens, and the thicknesses of TGO layer for the TBCs with 204 C-NS and 204 NS were measured as in the ranges of 5-9 and 3-7 μm, respectively. In the thermal shock test, the advantage of vertical cracks for thermal durability of TBC could be well investigated, showing relatively longer sustained cycles in the TBCs with vertical cracks. The TBCs with vertical cracks are more efficient in improving thermal durability than those without vertical cracks in cyclic thermal exposure.

1. Introduction

Thermal barrier coatings (TBCs) have been developed to protect metallic components in various engineering applications such as gas turbines, diesel engines, rocket engines, nuclear reactors, etc. TBC can be considered as a three-layer system, which consists of (1) metallic substrate; (2) oxidation-resistant metallic bond coat, usually MCrAlY (M = Co, Ni) or a platinum aluminide coating; and (3) ceramic top coat, usually from 7 to 8 wt.% yttria (Y_2O_3)-stabilized zirconia (ZrO_2). The top coat should have excellent thermal shock resistance, low thermal conductivity, and relatively high coefficient of thermal expansion (CTE) (Ref [1], [2]). The top coat is usually prepared using either air plasma-sprayed (APS) or electron-beam physical vapor deposition (EB-PVD) methods, while the bond coat is either diffusion-type coatings with nickel aluminide with doping of Pt-group elements or MCrAlY type overlay coatings. The MCrAlY bond coat is prepared using the APS, high-velocity oxygen fuel (HVOF) spray, or low-pressure plasma spray (LPPS) methods (Ref [3]). The bond coat provides a rough surface for the mechanical bonding of top coat, protects the underlying substrate against the high-temperature oxidation corrosion, and reduces the CTE mismatch between the substrate and the top coat. Many techniques such as EB-PVD, solution precursor plasma spray (SPPS), and APS methods are being used to obtain a good microstructure and hence to enhance thermal durability and mechanical properties of top coat in TBC system (Ref [1], [2], [4-6]). Among these techniques, the APS is preferred commercially because of its economic benefits, in contrast to the use of the complex and expensive EB-PVD (Ref [7-9]). TriplexPro™-200 system has been launched to offer an advanced TBC performance resulting from higher particle velocity, lower particle oxidation, and higher coating density, compared with the commercial APS system using 9 MB gun (Ref [10]). The particle velocity that can be produced in the TriplexPro™-200 is up to 560 m/s, which is of nearly HVOF quality with the particle velocity of about 700 m/s, and that in the conventional APS system (9 MB) is 350 m/s.

Zhe Lu, Sang-Won Myoung, Hyun-Sung Kim, Min-Sik Kim, Je-Hyun Lee, and **Yeon-Gil Jung**, School of Nano & Advanced Materials Engineering, Changwon National University, Changwon, Kyungnam 641-773, Republic of Korea; **Jung-Chel Jang**, Korea Electric Power Research Institute, Korea Electric Power Corporation, Daejeon 305-760, Republic of Korea; and **Ungyu Paik**, Department of Energy Engineering, Hanyang University, Seoul 133-791, Republic of Korea. Contact e-mails: lz19870522@126.com, jungyg@changwon.ac.kr, and upaik@hanyang.ac.kr.

Numerous factors have to be considered in practical applications of TBC, including high melting point, thermal stability, low thermal conductivity, chemical inertness, CTE match and good adhesion with the metallic substrate, low sintering rate, and thermo-mechanical properties (Ref 11). Among them, the thermal stability or durability in high-temperature environments, especially in cyclic thermal exposure, is essential factor to improve the reliability and lifetime performance of the APS-TBC system, and the thermal durability of TBC is closely related with its microstructure. There are three ways to enhance TBC performance, specially focused on the lowering of thermal conductivity of TBC: (1) studying about coating materials having a low thermal conductivity, (2) controlling the porosity in TBC, and (3) increasing the thickness of TBC. The effects of porosity and material on thermal conductivity of TBC have been reported, indicating that thermal conductivity is strongly dependent on the porosity and material composition (Ref 12). When the thicknesses of TBCs using APS are greater than 1.5 mm, the TBCs spontaneously fail during preparation or service (Ref 13-15), which makes other coatings or processes preferable, such as a dense vertical crack (DVC) TBC, gradient or high-porosity coatings, SPPS process, etc. (Ref 13, 16-19).

In general, the thermal and residual stresses are generated during preparation of TBCs and during cyclic thermal exposure, which result in spallation of top coat. Normally, the reported compressive residual stresses on thermal barrier-coated high-pressure turbine blade are in the ranges of 2.4-2.8 GPa for the as-prepared and 2.3-3.1 GPa after service, depending on surface geometries of thermally grown oxides (TGOs) (Ref 20). Also, the TGO layer develops large compressive stress upon cooling from operating temperatures, because of the substantial thermal expansion misfit with the underlying superalloy component (Ref 14, 15). Therefore, the stresses are mainly responsible for TBC failure. The APS-TBCs are prone to large scale spallation as the cracks induced due to thermal stresses propagate leading to failure. To release thermal stress mismatch, vertical type cracks are deliberately introduced in the top coat, thus reducing tendency of top coat to crack and buckle (Ref 21).

Therefore, in this study, thermomechanical properties of ZrO_2-based top coat with vertical type cracks were characterized, even though all the methods mentioned previously should be considered to design a new TBC. The microstructure of top coat was designed by developing the vertical type cracks as a new strategy for the advanced TBC, using an APS Triplex-Pro™-200 system. Two kinds of powder have been employed to prepare the top coat with vertical type cracks, and its microstructure evolution and thermal durability were investigated through the cyclic thermal exposure and thermal shock tests, including the delamination behavior or fracture behavior of TBC system to understand the effects of vertical cracks created on the top coat of TBCs. The relationship between thermal durability and starting powder (feedstock) was discussed, based on the microstructural and hardness variation before and after cyclic thermal exposure.

2. Experimental Procedure

2.1 Preparation of TBC

The vertical-cracked TBCs employed in this study were prepared using a specialized APS coating system (TriplexPro™-200, Sulzer Metco Holding AG, Switzerland). Ni-based superalloy (Nimonic 263, a nominal composition of Ni-20Cr-20Co-5.9Mo-0.5Al-2.1Ti-0.4Mn-0.3Si-0.06C in wt.%, ThyssenKrupp VDM, Germany) was used a substrate, which was disk shape (25.4 mm diameter and 5 mm thick). The substrate was sand blasted using an alumina powder and then the APS processes were conducted within 2 h. The APS process was applied to deposit a bond coat with a thickness of 300 ± 50 μm onto the substrate, using a Ni-based intermetallic powder (AMDRY 962, Sulzer Metco Holding AG, Switzerland). The nominal composition of AMDRY 962 is Ni-22Cr-10Al-1.0Y in wt.% and the particle size is in range of 56-106 μm. A top coat with a thickness of 600 ± 50 μm was air-plasma sprayed onto the bond coat, using powdered ZrO_2 containing 7-8 wt.% Y_2O_3. Two kinds of feedstock powder, METCO 204 C-NS (hereinafter C-NS; Sulzer Metco Holding AG, Switzerland, particle size of 45-125 μm) and METCO 204 NS (hereinafter NS, Sulzer Metco Holding AG, particle size of 11-125 μm), were used as the top coat (Ref 22). The deposition parameters of the bond and top coats are given in Table 1, and these parameters were selected from conditions indicated by the manufacturer of powders trying to guarantee the best deposition characteristics. The microstructure of TBC was controlled by reheating the surface of top coat using a plasma flame without powder feeding for five passes with the gun's moving speed of 500 mm/s at the distance of 50 mm using same equipment. The temperatures on the surface and bottom of specimen in the reheating process were measured using a Labview (Laboratory Virtual Instrumentation Engineering Workbench) system. The reheating process was conducted after natural air cooling the TBC at room temperature for 20 min. The reheating process was done within 25 min, including the cooling time after the top coat spraying. As a result, vertical type cracks were created on the top coat.

2.2 Microstructure and Characterization

The specimens with and without the vertical cracks were pre-processed to observe the cross-sectional microstructure and to measure the mechanical property. The mounted specimens were polished with the 3 and 1 μm diamond pastes. The cross-sectional view of microstructure was observed using a scanning electron microscope (SEM, JEOL Model JSM-5610, Japan). The thickness of the TGO layer formed at the interface between the bond and top coats after cyclic thermal exposure was measured using a SEM. Here, the mean thickness of the TGO was defined as an average of the thickness measured in 20 positions of the TGO. The measurement was done by every 30 μm along the interface direction using image obtained by a SEM. Image analysis was conducted on a

Table 1   The coating parameters for preparing the bond and top coats

Coating parameters	Bond coat	Top coat	Top coat
Classified powder	AMDRY 962	204 C-NS	204 NS
Powder feeding rate	90 g/min	100 g/min	75 g/min
Powder carrier gas	3 L/min	3.5 L/min	3.5 L/min
Gun distance	180 mm	150 mm	150 mm
Gun current/voltage	450 A/90 V	540 A/99 V	540 A/99 V
Gun speed	500 mm/s	500 mm/s	500 mm/s
Argon content/flow rate	30/20 NLPM	45/5 NLPM	45/5 NLPM
Step distance	8 mm	5 mm	5 mm

cross-sectional plane, using Image-Pro Plus software (Media Cybernetics, USA), and then the defects created in each TBC were classified with the horizontal and vertical cracks, and pore. The hardness values of top coat were determined using a Vickers indenter (HM-114, Mitutoyo Corp., Japan) with a load of 10 N, using the equation proposed by Lawn (Ref 23). The dwell time was 10 s. To obtain more reliable values, 10 points were indented for each result. The impression size was measured by SEM, and all experiments were performed in air and at room temperature.

2.3 Thermal Cycling Test and Thermal Shock Test

The cyclic thermal exposure tests were performed for 381 cycles in the specially designed furnace: one side of specimen was exposed and the other side air-cooled. The surface temperature of specimen is about 1100 °C with a temperature difference of 150 °C between the top surface and bottom of specimen with a dwell time of 60 min, followed by natural air cooling for 10 min at room temperature. The failure criterion was defined as 25% buckling or spallation of the top coat area. Specimens were removed at different fractions of their life for cross-sectional studies, while others were observed for signs of failure and were cycled until the failure criterion was met. The specimens for the thermal shock tests were heated in a muffle furnace. When the temperature of the furnace reached 1100 °C, the specimens were pushed into the furnace. In the thermal shock tests, the specimens were held for about 25 min in the furnace and then directly quenched in water for 5 min. The temperatures of water throughout the thermal shock tests was maintained between 20 and 35 °C. More than 50% of the spalled region in the surface of top coat was adopted as criterion for the failure in water-quenched specimens. The thermal shock tests were reported in previous studies while investigating the thermal durability of TBC system (Ref 24-27). At least five specimens were tested for each condition.

3. Results and Discussion

3.1 Microstructure of As-Prepared Specimens

The top coats were well deposited with the designed concept, showing the dense and porous cross-sectional microstructures with feedstock species. The bond and top coats of 350 ± 50 and 600 ± 50 μm, respectively, were well developed by changing the number of coating passes and the spray parameters. The microstructure of top coat prepared with 204 C-NS (Fig. 1a-1) is relatively porous, compared with 204 NS (Fig. 1b-1). There are relatively large defects such as global pores and unmelted particles, especially in the porous microstructure prepared with 204 C-NS. These defects will accelerate crack propagation and reduce the mechanical properties such as hardness and adhesive strength, resulting in the deterioration of thermal durability of TBC system in thermal exposure. However, these are general defects observed in the microstructure of TBC prepared using the APS system. The porosities in the top coats observed for 204 C-NS and 204 NS were about 17 and 10%, respectively. In this study, defect species were classified in terms of pores, horizontal defects, and vertical defects to confirm the differences in microstructures with feedstock species. The pores constituted a large portion in total porosity obtained in the image analysis, especially in the case of top coat prepared with 204 C-NS. The particle sizes of 204 C-NS and 204 NS are 45-125 and 11-125 μm, respectively. The larger particle size and narrower particle size distribution of 204 C-NS could influence the microstructure, because the feedstock powder with larger particle size does not easily melt due to the nature of APS process. The changes in powder feeding rates in the spray parameters could also influence the microstructure. The developed microstructure of top coat with vertical cracks could be well controlled as shown in Fig. 1(a-2) and (b-2). The developed vertical cracks are indicated with arrows. The average number of cracks in the top coats prepared with 204 C-NS and 204 NS was 37 and 53 per inch, respectively. The temperatures measured on the top coat and bottom of specimen were 1700-1900 °C and about 280 °C, respectively, during the reheating process. After finishing the reheating process, the surface temperature range of top coat was 400-500 °C. In the case of same feedstock, the microstructures of TBC specimens with vertical cracks were denser than those without vertical cracks, especially on the surface, owing to the densification during reheating process onto the surface for developing vertical cracks. It can be verified in the hardness values measured for each TBC with and without vertical cracks.

3.2 Cyclic Thermal Exposure Test

The cross-sectional microstructures of TBCs which survived after the thermal exposure of 381 cycles (8000
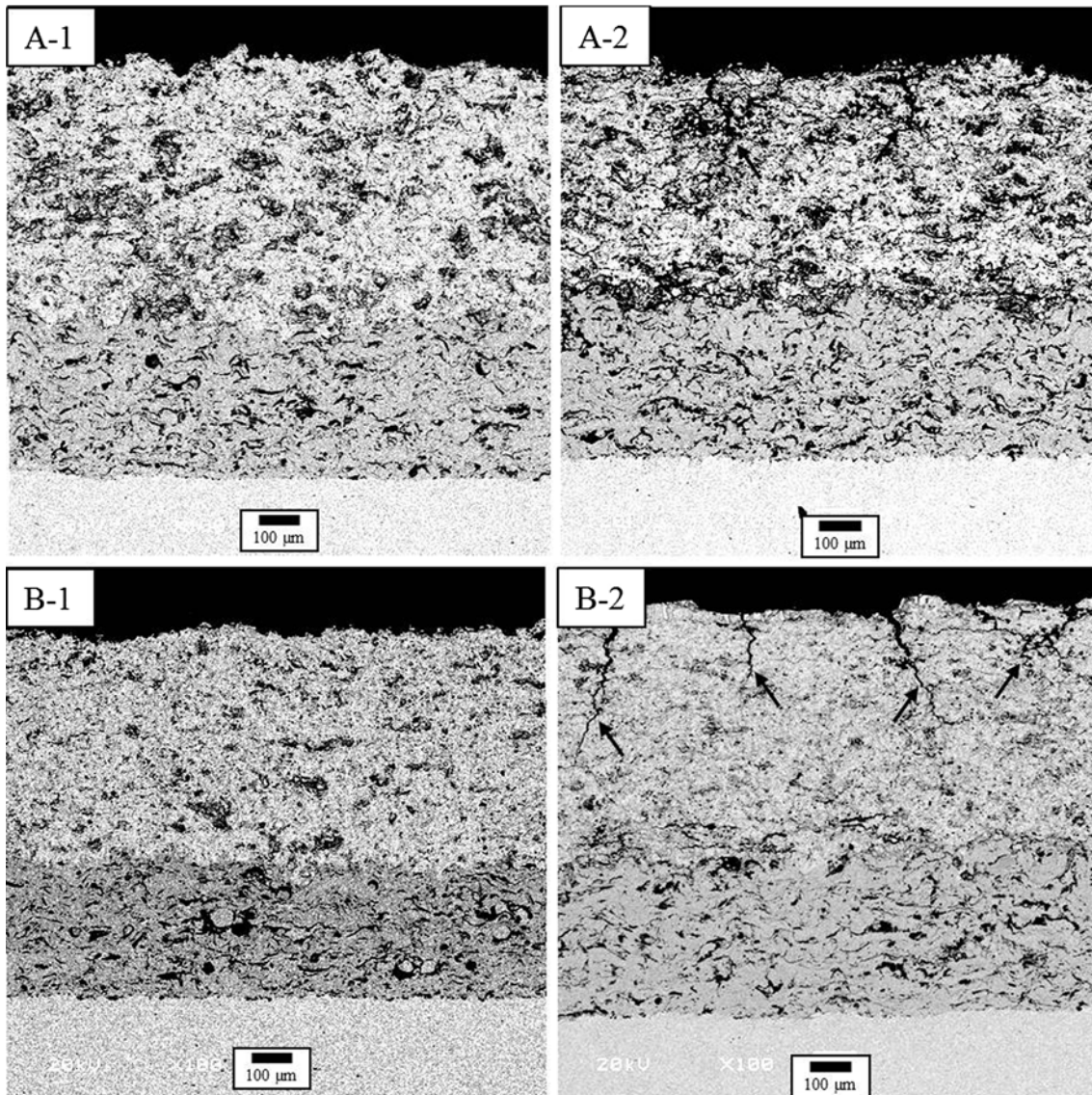
Fig. 1 Cross-sectional microstructures of as-prepared TBCs; (a) TBC with 204 C-NS and (b) TBC with 204 NS. Each number indicates microstructures without and with vertical cracks, respectively. Arrows indicate the developed vertical cracks

EOH) are shown in Fig. 2. Equivalent operating hour (EOH), usually used in ALSTOM™ and ABB™ for the maintenance and inspection of gas turbines, is a function of the operating hours, coefficient of correction, load rejection, equivalent hours for startup, trips, rapid load change, standby, fuel operation, etc. (Ref 28, 29). The maintenance and inspection interval units are performed based on the EOH rather than on the actual running hours:

$$EOH = AOH + 20[\Sigma S_i + \Sigma LR_i + \Sigma T_i + \Sigma LC_i] \times F,$$
(Eq 1)

where EOH, AOH, ΣS_i, ΣLR_i, ΣT_i, ΣLC_i, and F represent the equivalent operating hours, actual operating hours, coefficient of correction, load rejection, trip, rapid

load change, and fuel factor (gas: 1.0), respectively. In this study, EOH was estimated as an approximate value, multiplying 21 by the number of cycle.

In the cyclic thermal exposure tests, the TBCs using 204 C-NS powder showed a sound condition at the interface between the bond coat and top coat without any cracking or delamination up to 381 cycles, as shown in Fig. 2(a-1) and (a-2), independent of vertical cracks. After the tests, the specimens showed relatively denser microstructures than the as-prepared specimens, owing to re-sintering through the thermal exposure for 381 cycles. The TBC without vertical cracks prepared with 204 NS was delaminated after 250-270 cycles (5250-5670 EOH). However, the TBC with vertical cracks prepared with 204 NS showed a sound condition at the interface between the bond and top coats after 381 cycles (Fig. 2b), and no cracking was observed at the interface microstructure.
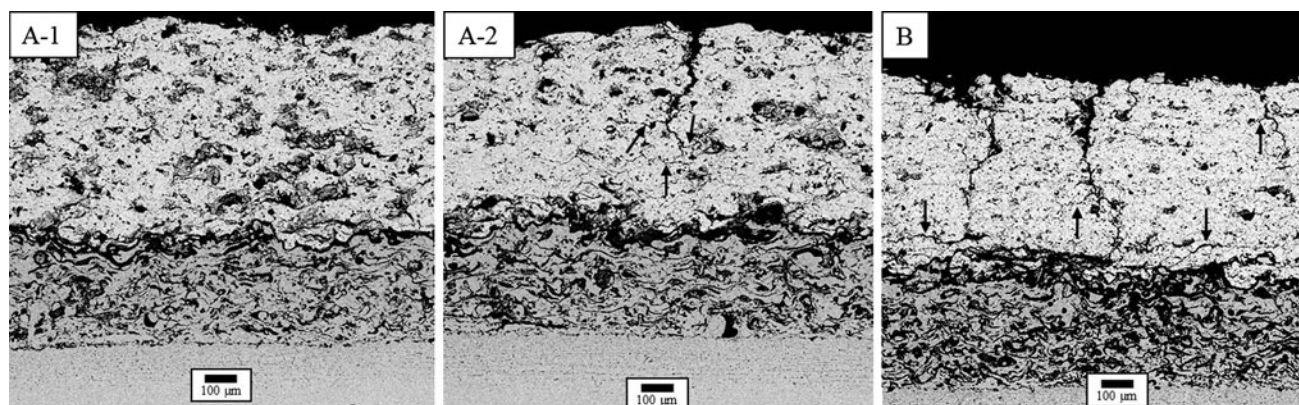
Fig. 2 Cross-sectional microstructures of TBCs survived after the thermal exposure for 381 cycles (8000 EOH); (a) TBC with 204 C-NS and (b) TBC with 204 NS. Each number indicates microstructures without and with vertical cracks, respectively. Arrows indicate the newly developed and/or integrated horizontal cracks after thermal exposure

After thermal exposure, all vertical cracks increased in length, and the small horizontal cracks were integrated into the long and thick horizontal cracks, indicating the improved thermal durability of the TBCs with vertical cracks. The newly developed and/or integrated horizontal cracks after thermal exposure were indicated with arrows. However, all vertical cracks did not traverse through the entire thickness of the coating. The microstructural analysis for the top coats with and without vertical cracks revealed different porosities with feedstock species after the thermal exposure of 381 cycles, as shown in Table 2, which corresponded well with the microstructural features observed in Fig. 1 and 2.

The improvement of thermal durability in the TBCs with vertical cracks could be well observed in the magnified interface microstructure. The interface microstructures between the bond and top coats of the TBCs with vertical cracks before and after cyclic thermal exposure are shown in Fig. 3. The interfaces between the top and bond coats in all kinds of as-prepared TBCs showed a sound condition without any global defects and without TGO layer. After the thermal exposure for 381 cycles, the thickness of TGO layer was measured as 5-9 and 3-7 μm for TBCs obtained with 204 C-NS and 204 NS, respectively: the TGO layer exhibited an irregular shape on both sides of the top and bond coats, and the interface microstructures still show a sound condition without any delamination or cracking. In the APS process, lots of small particles accelerated by the high-power plasma or combustion impinge on the bond coat to form top coat. Thus, TBCs prepared by the APS show the undulated microstructure at the interface between the bond and top coats, as shown in Fig. 3. If the thickness of TGO layer is greater than 10 μm, the interface between the TGO layer and the top coat normally starts to delaminate and show a failure phenomenon (Ref 5, 30, 31). The TGO growth is more related to the bond coat properties and chemistry as ZrO_2 is transparent at high temperature. In this study, the compositions of bond coats were the same in both TBCs, and the vertical cracks did not reach at the interface. Therefore, it can be presumed that one of causes for the difference in the thickness of TGO layer is the microstructure of top coat. However, a reason might be the different levels of dispersion at the interface (in both the bond and top coats) of the TGO, and thus not only did it become more difficult to measure or evaluate the real TGO thickness but also caused the coatings with a better accumulation of the TGO in layered structures to fail earlier. As a result, the microstructure's control including vertical cracks is important for improving thermal durability as well as TGO growth in a dense TBC, because the strain tolerance will get deteriorated and the CTE mismatch between the top and bond coats will be increased as well, resulting in crack initiation and growth.

3.3 Thermal Shock Test

The thermal shock tests were performed on the four different specimens with and without vertical cracks. The number of sustained cycles for each TBC with and without vertical cracks in the thermal shock tests is shown in Fig. 4. Two specimens with and without vertical cracks were prepared with 204 C-NS powder. The specimens with vertical cracks were delaminated in range of 114-126 cycles, whereas the specimens without vertical crack were delaminated in range of 63-97 cycles. Similarly, two different specimens with and without vertical cracks were prepared with 204 NS powder. The specimens with vertical cracks powder started to delaminate after 40 cycles, and more than 50% delamination occurred in range of 48-56 cycles, while the specimens without vertical cracks initiated the delamination after 15 cycles and completely spalled in range of 20-50 cycles. The lower number of sustained cycles for TBCs prepared with 204 NS in the thermal shock tests might be due to the high level of residual stresses due to the relatively dense microstructure. These results are consistent with those of other investigators, in that partially stabilized zirconia layers thicker than 300 μm are more susceptible to cracking and delamination (Ref 32).

The cross-sectional microstructures of TBCs after the thermal shock tests are shown in Fig. 5. In all specimens

Table 2 Microstructural analysis for top coats prepared with 204 C-NS and 204 NS after thermal exposure

Microstructural parameters	TBC with 204 C-NS (without vertical crack)	TBC with 204 C-NS (with vertical crack)	TBC with 204 NS (with vertical crack)
Total porosity from image analysis, %	12.6	9.6	8.9
Fraction of horizontal defects in porosity, %	0.6	2.1	1.7
Fraction of horizontal defects in porosity, %	0.3	1.6	2.4
Fraction of pores in porosity, %	11.6	6.0	4.8
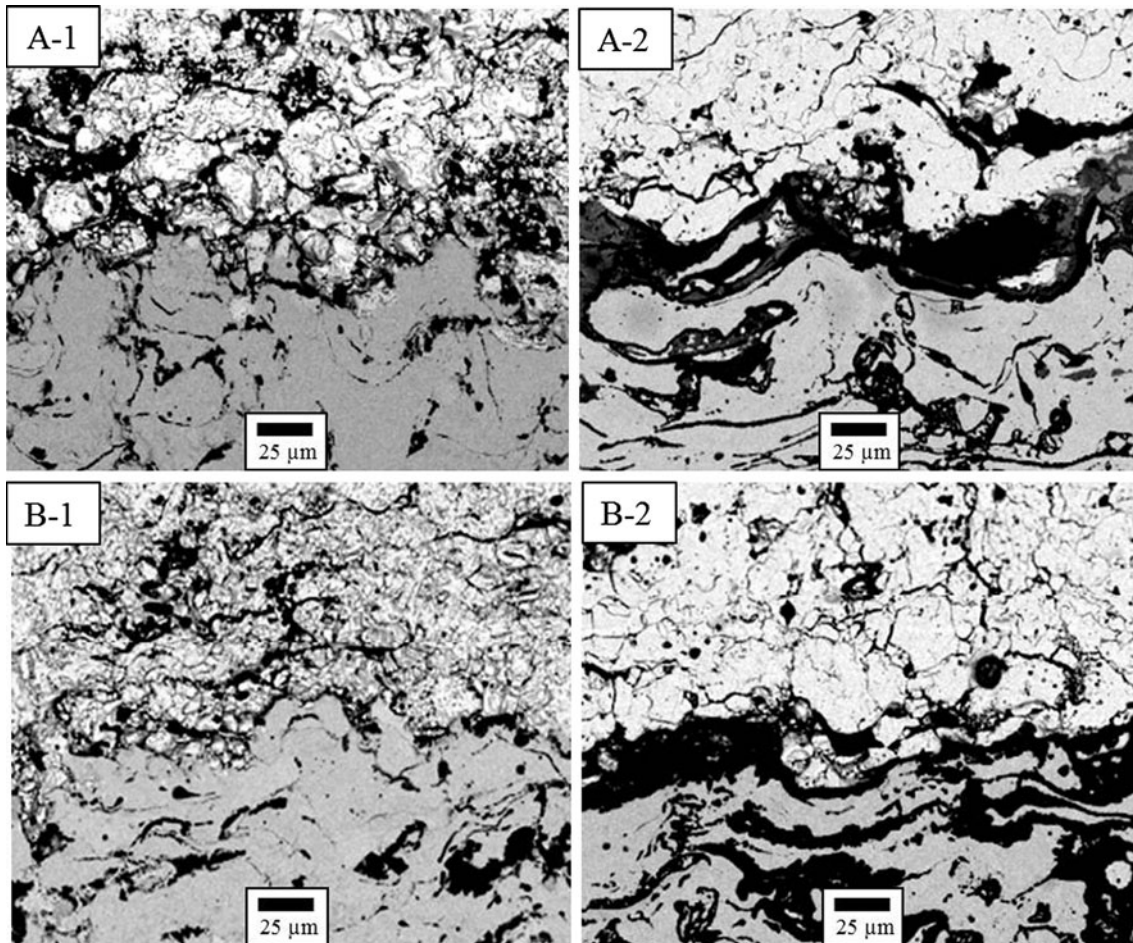
Fig. 3 Cross-sectional microstructures at each interface between the top and bond coats in TBCs with vertical cracks before and after the thermal exposure for 381 cycles; (a) TBC with 204 C-NS and (b) TBC with 204 NS. Each number indicates microstructures before and after cyclic thermal exposure, respectively

after the thermal shock tests, the spalling modes were similar, as shown in Fig. 5, showing a complete delamination at the interface between the bond and top coats. The possible explanation might be the large temperature difference between the substrate and the surface of top coat in the quenching and heating times. In the case of TBCs without vertical cracks, the temperature difference increased, and as a result, more thermal stresses developed at the interface of the bond and top coats. The mismatch of CTE between the top and bond coats or the oxidation of bond coat leads to failure. The other possible explanation might be that elastic strain energy storage was more in the top coat without vertical cracks than that with vertical cracks, which could be the driving force for debonding or spalling of the top coat. The bond coat in all specimens after the thermal shock tests showed lots of visible defects and more oxide contents than that of the as-prepared specimens.

3.4 Mechanical Properties

The hardness values of top coats before and after cyclic thermal exposure were measured using Vickers indentation as a function of thermal exposure cycle. The results are shown in Fig. 6. The indentation tests were carried out on the sectional plane with loads of 10 N. The hardness

values of TBCs with and without vertical cracks for the as-prepared with 204 C-NS were determined to be 4.5 ± 0.3 and 4.2 ± 0.2 GPa (mean $\pm$ standard deviation), respectively. The hardness values were determined to be 5.8 ± 0.2 and 4.0 ± 0.2 GPa for the TBCs with and without vertical cracks, respectively, after the thermal exposure to 381 cycles. In the case of TBCs with and without vertical cracks for the as-prepared with 204 NS, the corresponding hardness values were determined to be 7.8 ± 0.4 and 6.5 ± 0.3 GPa, respectively. After the thermal exposure for 381 cycles, the hardness value of

TBC with vertical cracks was determined to be 8.4 ± 0.3 GPa. The TBC without vertical cracks delaminated in range of 250-270 cycles. Therefore, the hardness value was not determined.

The hardness values obtained in the top coats with and without vertical cracks were higher than those of top coats previously reported, with nominal values of 3.2 and 4.4 GPa for the TBCs with the 204 C-NS and 204 NS powders, respectively (Ref 33, 34). However, it is hard to confirm the above because the hardness value is strongly dependent on microstructural feature in TBC and measured on the
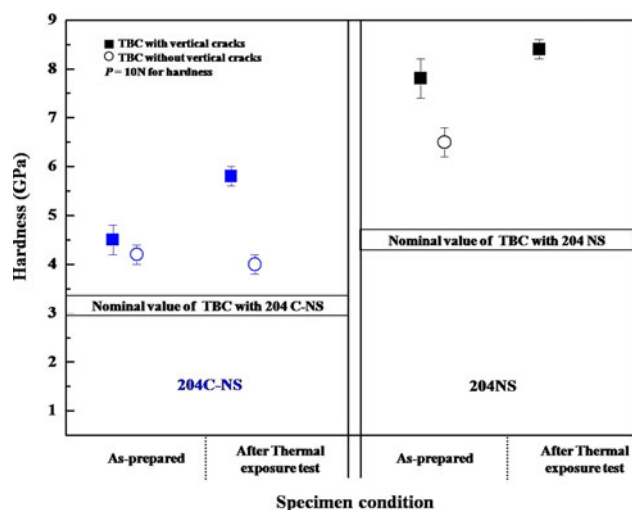

Fig. 4 Number of sustained cycles for delamination of top coat in the thermal shock tests. Closed and open bars indicate the number of sustained cycles for delamination or spalling of top coat in TBCs with and without vertical cracks, respectively

Fig. 6 The hardness values of top coats before and after the thermal exposure for 381 cycles. Indentation for hardness was conducted on the sectional plane at 10 N. Closed and open marks indicate the hardness values of TBCs with and without vertical cracks, respectively
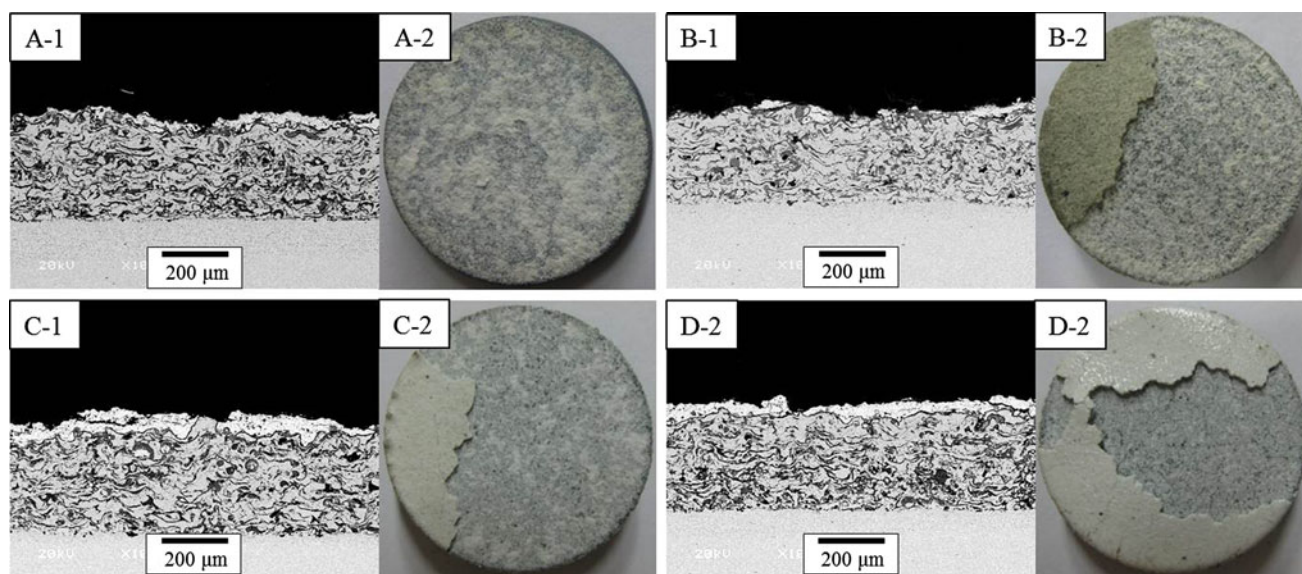

Fig. 5 Cross-sectional microstructures and surface micrographs of TBCs with and without vertical cracks after the thermal shock tests; (a) TBC with vertical cracks using 204 C-NS, (b) TBC without vertical cracks using 204 C-NS, (c) TBC with vertical cracks using 204 NS, and (d) TBC without vertical cracks using 204 NS. Each number indicates the cross-sectional microstructures and surface micrographs of delaminated TBCs, respectively

regions without defects. The hardness values of TBCs as-prepared with 204 NS were increased with the development of vertical cracks, while the hardness value of TBC as-prepared with 204 C-NS did not change much with the development of vertical cracks, indicating that the reheating process is more efficient in improving mechanical property in a dense microstructure. The hardness values measured were in good agreement with the microstructural evolution shown in Fig. 2. The microstructure was densified owing to re-sintering through the thermal exposure for 381 cycles, resulting in disappearance of pores and "splat" boundaries. The microstructure increased the hardness values of TBCs after cyclic thermal exposure.

4. Conclusions

The microstructure of TBCs could be controlled well by changing feedstock powder in the TriplexPro-200 system, showing the dense, porous, and vertical-cracked microstructures in the top coat. The TBC without vertical cracks prepared with 204-NS powder was delaminated in range of 250-270 cycles. The TBCs with and without vertical cracks prepared with 204 C-NS powder and the TBC with vertical cracks prepared with 204 NS survived after the thermal exposure for 381 cycles, and no cracking or delamination at the interface between the bond and top coasts was observed. The thicknesses of TGO layer for the TBCs with 204 C-NS and 204 NS were measured to be in ranges of 5-9 and 3-7 μm, respectively, showing the effect of microstructure. The TBCs without vertical cracks prepared with 204 C-NS and 204 NS initiated the delamination in ranges of 63-97 and 20-50 cycles, respectively, while those with vertical cracks in the ranges of 114-126 and 48-56 cycles, respectively. The cyclic thermal exposure and thermal shock tests revealed that the microstructure's control including vertical cracks are important in enhancing the thermal durability. The hardness values of TBCs without vertical cracks as-prepared with 204 C-NS and 204 NS were determined to be 4.2 ± 0.2 and 6.5 ± 0.3 GPa, respectively, and those of TBCs with vertical cracks were 4.5 ± 0.3 and 7.8 ± 0.3 GPa, respectively. After cyclic thermal exposure, the TBCs with vertical cracks were increased to 5.8 ± 0.2 and 8.4 ± 0.2 GPa in both TBCs obtained with 204 C-NS and 204 NS, respectively. These evidences allow us to control the thermomechanical properties of TBC and propose the efficient coating in protecting the substrate from both thermal and mechanical environments.

References

1. A.G. Evans, D.R. Mumm, J.W. Hutchinson, G.H. Meier, and F.S. Pettit, Mechanisms Controlling the Durability of Thermal Barrier Coatings, *Prog. Mater. Sci.*, 2001, **46**, p 505-553

2. N.R. Padture, M. Gell, and E.H. Jordan, Thermal Barrier Coatings for Gas-Turbine Engine Applications, *Science*, 2002, **296**, p 280-284

3. J.H. Zaat, A Quarter of Century of Plasma Spraying, *Annu. Rev. Mater. Sci.*, 1983, **13**, p 9-42

4. D.R. Clarke and S.R. Phillport, Thermal Barrier Coating Materials, *Mater. Today*, 2005, **8**(6), p 22-29

5. J.Y. Kwon, J.H. Lee, Y.G. Jung, and U. Paik, Effect of Bond Coat Nature and Thickness on Mechanical Characteristic and Contact Damage of Zirconia-Based Thermal Barrier Coatings, *Surf. Coat. Technol.*, 2006, **201**, p 3483-3490

6. J.Y. Kwon, J.H. Lee, H.C. Kim, Y.G. Jung, U. Paik, and K.S. Lee, Effect of Thermal Fatigue on Mechanical Characteristics and Contact Damage of Zirconia-Based Thermal Barrier Coatings with HVOF-Sprayed Bond Coat, *Mater. Sci. Eng. A*, 2006, **429**, p 173-180

7. D.R. Clarke and C.G. Levi, Materials Design for the Next Generation Thermal Barrier Coating, *Annu. Rev. Mater. Res.*, 2003, **33**, p 383-417

8. H.-J. Rätzer-Scheibe, U. Schulz, and T. Krell, The Effect of Coating Thickness on the Thermal Conductivity of EB-PVD PYSZ Thermal Barrier Coatings, *Surf. Coat. Technol.*, 2006, **201**, p 5636-5644

9. J.R. Nicholls, K.J. Lawson, A. Johnstone, and D.S. Rickerby, Methods to Reduce the Thermal Conductivity of EB-PVD TBCs, *Surf. Coat. Technol.*, 2002, **151-152**, p 383-391

10. K. Richardt, K. Bobzin, D. Sporer, T. Schläfer, and P. Fiala, Tailor-Made Coatings for Turbine Applications Using the Triplex Pro 200, *J. Therm. Spray Technol.*, 2008, **17**, p 612-616

11. X.Q. Cao, R. Vassenb, and D. Stoeverb, Ceramic Materials for Thermal Barrier Coatings, *J. Eur. Ceram. Soc.*, 2004, **24**, p 1-10

12. R. Dutton, R. Wheeler, K.S. Ravichandran, and K. An, Effect of Heat Treatment on the Thermal Conductivity of Plasma-Sprayed Thermal Barrier Coatings, *J. Therm. Spray Technol.*, 2000, **9**, p 204-209

13. T. Bhatia, A. Ozturk, L. Xie, E.H. Jordan, B.M. Cetegen, M. Gell, X. Ma, and N.P. Padture, Mechanisms of Ceramic Coating Deposition in Solution-Precursor Plasma Spray, *J. Mater. Res.*, 2002, **17**, p 2363-2372

14. W. Schlichting, N.P. Padture, E.H. Jordan, and M. Gell, Failure Modes in Plasma-Sprayed Thermal Barrier Coatings, *Mater. Sci. Eng. A*, 2003, **342**, p 120-130

15. A. Rabiei and A.G. Evans, Failure Mechanism Associated with the Thermally Grown Oxide in Plasma-Sprayed Thermal Barrier Coatings, *Acta Mater.*, 2000, **48**, p 3963-3976

16. T.A. Talyor, US Patent No. 5073433, 1991

17. A.D. Jadhav, N.P. Padture, E.H. Jordan, M. Gell, P. Miranzo, and E.R. Fuller, Jr., Low-Thermal-Conductivity Plasma-Sprayed Thermal Barrier Coatings with Engineered Microstructures, *Acta Mater.*, 2006, **54**, p 3343-3349

18. A. Jadhav, N.P. Padture, F. Wu, E.H. Jordan, and M. Gell, Thick Ceramic Thermal Barrier Coatings with High Durability Deposited Using Solution-Precursor Plasma Spray, *Mater. Sci. Eng. A*, 2005, **405**, p 313-320

19. T.A. Taylor, D.L. Appleby, A.E. Weatherill, and J. Griffiths, Plasma-Sprayed Yttria-Stabilized Zirconia Coatings: Structure-Property Relationships, *Surf. Coat. Technol.*, 1990, **43-44**, p 470-480

20. Y.H. Sohn, E.Y. Lee, B.A. Nagaraj, R.R. Biederman, and R.D. Sisson, Jr., Microstructural Characterization of Thermal Barrier Coatings on High Pressure Turbine Blades, *Surf. Coat. Technol.*, 2001, **146-147**, p 132
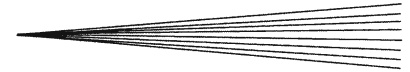
21. M. Madhwal, E.H. Jordan, and M. Gell, Failure Mechanisms of Dense Vertically-Cracked Thermal Barrier Coatings, *Mater. Sci. Eng. A*, 2004, **384**, p 151-161

22. Sulzer-Metco Thermal Spray Materials Guide, http://www.sulzermetco.com/

23. B.R. Lawn, *Fracture of Brittle Solids*, 2nd ed., Cambridge University Press, Cambridge, UK, 1993

24. C. Zhou, N. Wang, Z. Wang, S. Gang, and H. Xu, Thermal Cycling Life and Thermal Diffusivity of a Plasma-Sprayed Nanostructured Thermal Barrier Coating, *Scripta Mater.*, 2004, **51**, p 945-948

25. P.K. Panda, T.S. Kannan, J. Dubois, C. Olagnon, and G. Fantozzi, Thermal Shock and Thermal Fatigue Study of Ceramic Materials on a Newly Developed Ascending Thermal Shock Test Equipment, *Sci. Technol. Adv. Mater.*, 2002, **3**, p 327-334

26. S.O. Chwa and A. Ohmori, Microstructures of ZrO_2-8wt.%Y_2O_3 Coatings Prepared by a Plasma Laser Hybrid Spraying Technique, *Surf. Coat. Technol.*, 2002, **153**, p 304-312

27. X.Q. Ma and M. Takemoto, Quantitative Acoustic Emission Analysis of Plasma Sprayed Thermal Barrier Coatings Subjected to Thermal Shock Tests, *Mater. Sci. Eng. A*, 2001, **308**, p 101-110

28. Y. Radin and T. Kontorovich, Equivalent Operating Hours Concept for CCPP Components Reliability Evaluation, *2012 International Conference on Power Energy System*, 2012, vol 13, p 175-178

29. GeneralCologne Re™, Power Re-View, https://www.facworld.com/WebLib.NSF/ObjectPreview/1Power2.pdf/$File/Power2.pdf

30. K. Ma and J.M. Schoenung, Isothermal Oxidation Behavior of Cryomilled NiCrAlY Bond Coat: Homogeneity and Growth Rate of TGO, *Surf. Coat. Technol.*, 2011, **205**, p 5178-5185

31. H.J. Jang, D.H. Park, Y.G. Jung, J.C. Jang, S.C. Choi, and U. Paik, Mechanical Characterization and Thermal Behavior of HVOF-Sprayed Bond Coat in Thermal Barrier Coatings (TBCs), *Surf. Coat. Technol.*, 2006, **200**, p 4355-4362

32. P.G. Tsantrizos, G.E. Kim, and T.A. Braezinski, TBCs on Free Standing Multilayer Components, *AGARD SMP Meeting on "Thermal Barrier Coatings"* (Aalberg, Denmark), 1997, p 7-1-7-8

33. P.H. Lee, S.-Y. Lee, J.-Y. Kwon, S.W. Myoung, J.H. Lee, Y.G. Jung, H. Cho, and U. Paik, Thermal Cycling Behavior and Interfacial Stability in Thick Thermal Barrier Coatings, *Surf. Coat. Technol.*, 2010, **205**, p 1250-1255

34. S.W. Myoung, J.H. Kim, W.R. Lee, Y.G. Jung, K.S. Lee, and U. Paik, Microstructure Design and Mechanical Properties of Thermal Barrier Coatings with Layered Top and Bond Coats, *Surf. Coat. Technol.*, 2010, **205**, p 1229-1235